Journal of Solid Mechanics Vol. 16, No. 1 (2024) pp. 97-119
DOI: 10.60664/jsm.2024.3091790

Research Paper

Size-Dependent Buckling Analysis of Three-Layered Nano-Plate on Orthotropic Foundation Using Surface Theory

A.H. Soltan Arani [1], A. Ghorbanpour Arani [1,2*] , Z. Khoddami Maraghi [3]

[1] *Department of Solid Mechanics, Faculty of Mechanical Engineering, University of Kashan, Kashan, Iran*
[2] *Institute of Nanoscience & Nanotechnology, University of Kashan, Kashan, Iran*
[3] *Faculty of Engineering, Mahallat Institute of Higher Education, Mahallat, Iran*

Received 11 September 2023; Received in revised form 20 June 2024; Accepted 24 June 2024

ABSTRACT

In this study, a nonlocal refined plate theory based on the stretching effect is extended to examine the buckling behavior of three-layered simply supported nanoplates resting on orthotropic foundation by taking into account the surface effects. The core properties are considered non-homogeneous properties based on the power-law distribution, which is gradually varying in the thickness direction of core. In this regard, due to the asymmetry of the material properties in the core thickness direction, the mid-plane of structure and the neutral plane is not coincided. Accordingly, it is necessary to consider the neutral surface concept and select it as the reference plane. The position of neutral surface is determined based on the nonlocal higher order shear deformation theory and then linear governing equilibrium equations are derived by employing the principle of minimum potential energy. On the other hand, face sheets are assumed using piezoelectric materials and considered as sensors and actuators. Eventually, Navier-type solution is utilized to obtain the analytical results of three-layered nano-plate subjected to electric field. In order to check the accuracy and efficiency of the current model, a validation study is carried out based on the obtained results and available results in the previous literature. The achieved results have a good agreement with the results in the previously published literature. Finally, the influences of different foundation, residual stress, surface effects, stretching effect, neutral surface, aspect ratio, thicknesses ratio, non-local parameter, length scale parameter, gradient index and initial voltage are examined on critical buckling load of sandwich nano-plate in details. Numerical results show that the residual surface stress and neutral surface position have an undeniable influence on the critical buckling load in the high thicknesses of nano-plate. It is expected that the results of current study to be utilized in designing micro/nano-electro-mechanical systems components based on smart nanostructures.

Keywords: Bi-axial buckling load; Neutral surface; Nonlocal strain gradient theory; Surface effects.

*Corresponding author. Tel.: +98 31 55913434; Fax: +98 31 55913444.
E-mail address: aghorabn@kashanu.ac.ir (A. Ghorbanpour Arani)

Copyright: © 2024 by the authors. Submitted for possible open access publication under the terms and conditions of the Creative Commons Attribution (CC BY) license (https://creativecommons.org/licenses/by/4.0/).

1 INTRODUCTION

DEVELOPMENT and advancement in various industries including aerospace and thermal power plants is caused that the requirement for materials with high thermal and mechanical strength is more taken into consideration than ever before. Functionally graded materials (FGM) are inhomogeneous materials including two or more various materials by varying the microstructure from one material to another material with a specific gradient. Their dating as an engineering concept reaches to the last quarter of the 20th century. The aircraft and aerospace industry, the computer circuit industry and the fabrication of electrical, electrochemical as well as biomaterials devices are examples of the use of these materials. FGMs as materials with improved properties have attracted the attention of many researchers [1-7]. Piezoelectric materials are materials that have the ability to generate internal electrical charge from applied mechanical stress. As well as in reverse direction, they can be created a strain when subjected to an electric field. These technologies are used as actuators and sensors due to the excellent mechanical properties and tunable electric properties in a wide range of the applied devices and products in modern societies especially. Thus far, many researchers have focused their research on studying and investigating the behavior of piezoelectric materials [8-13].

A multi-layered plate is a special form of a sandwich structure comprising a combination of different laminates which are bonded to each other so that its properties are considered as the properties of an integrated structure. The primary advantage of multi-layered plates is very high stiffness-to-weight and high bending strength-to-weight ratio. Lightweight and stiff laminated panels are vital elements of many modern civil, aircraft and spacecraft designs. Subsequently, researchers started to investigate the behavior of the multi-layered structures in the last few years.

Cao et al. [14] studied dynamic analysis of viscoelastically subjected to moving loads using multi-layer moving plate method. They extracted the governing equations of connected double-plate system by using Reissner-Mindlin plate theory. Ragb and Matbuly [15] introduced different numerical schemes to formulate and solve nonlinear vibration analysis of elastically supported multilayer composite plate resting on Winkler - Pasternak foundation by a first order shear deformation theory (FSDT). The obtained results show that the used method is an accurate efficient model in the dynamic analysis of discontinuity structure resting on nonlinear elastic foundation. Taghizadeh et al. [16] investigated mechanical behavior of a novel multi-layer sandwich panels subjected to indentation of a spherical indenter load experimentally and numerically. Amoozgar et al. [17] employed a combining a two-dimensional a one-dimensional nonlinear beam analysis to study the influences of initial curvature and lattice core shape on the vibration of sandwich beams. They used a time-space scheme to obtain nonlinear governing equations of the sandwich beam. Their results show that the lattice unit cell shape affects both in-plane and out of plane stiffness and result in changes the dynamic behavior of the beam. Sahoo et al. [18] predicted nonlinear vibration analysis of FGM sandwich structure under linear and nonlinear temperature distributions numerically using the higher-order shear deformation theory (HSDT). A parametric study on buckling behavior of sandwich beam consisting of a porous ceramic core including the effects of length-to-thickness ratio, volume fraction of FGM and various porosity patterns based on third-order shear deformation theory (TSDT) was presented by Derikvand et al. [19]. The governing equilibrium equations were solved for different end conditions using the differential transform method and physical neutral axis of the beam. Li et al. [20] used hyperbolic tangent shear deformation theory for analysis of free vibration of FG honeycomb sandwich plates with negative Poisson's ratio. They solved the derived governing dynamic equations by applying the Navier's method and fluid–solid interface conditions. The corresponding results display that the FG honeycomb core with negative Poisson's ratio can yield much lower frequencies. Instability analysis of axially moving sandwich plates with magnetorheological core and polymeric face sheets reinforced with graphene nanoplatelets by using FSDT were studied by Ghorbanpour Arani et al. [21]. The Halpin–Tsai model and the rule of mixture are utilized to estimate the effective mechanical properties. A novel unified model for vibration analysis of a thick-section sandwich structure was presented based on the variational asymptotic method by Li et al. [22]. They studied the effects of temperature gradients in the thickness direction, core thickness and boundary conditions by a detailed parametric study. Liu et al. [23] analyzed the buckling and vibration studies of the sandwich plates based on the isogeometric analysis in conjunction with the refined shear deformation theory.

Many researchers have studied the mechanical behavior of structures over the past centuries. Today, with the advancement of technology and the development of industries, achieving to the exact results requires the use of new models and methods. Laminated structures are used in many engineering industries. The different theories are used to simulate and obtain analytical results that the most common of these theories are Classical plate theory (CPT), FSDT and HSDT. As the thickness of the sheet increases, the accuracy of these theories decreases. Size effects play a significant role in predicting mechanical behavior when structure is being studied in a small scale. The best alternative approach to study the mechanical behavior of materials is the use of the continuum mechanics relationships. The effect of size is not taken into account in classical continuum mechanics theory. For this reason,

this theory cannot predict the mechanical behavior of nanostructures and micro-structures well. Various theories including Strain gradient theory (SGT) and Modified strain gradient theory (MSGT), Couple stress theory (CST) and Modified couple stress theory (MCST) is proposed in order to elimination of this defect. Layer-wise (LW) and zig-zag (ZZ) theories provide sufficiently accurate response for relatively thick laminated structures. These theories have the ability to capture the inter-laminar stress fields near the edges. Refined plate theories (RPT) are theories that assume the uniaxial and lateral displacements have bending and shear components. In them the bending and shear components do not contribute toward shear forces and bending moments, respectively. The most interesting feature of these theories is that they have high accuracy for a quadratic variation of the transverse shear strains across the thickness also satisfies the zero traction boundary conditions on the top and bottom surfaces of the plate without using shear correction factors. Several models of RPT with different form functions by dividing the transverse displacement into bending and shear parts for plate structures are proposed. Quasi-three-dimensional and Three-dimensional (3D) are the new contributions of the proposed theories which are compatible with the numerical method and naturally taken into account in the thickness direction. Examples of the use of these theories in the published articles are expressed as follows.

Ren et al. [24] derived the nonlocal strong forms for various physical models in traditional methods. They derived the nonlocal forms of electro-magneto-elasticity thin plate and phase-field fracture method based on nonlocal operator method by using the variational principle/weighted residual method. Pham et al. [25] studied the nonlocal dynamic response of sandwich nanoplates with a porous FG core using higher-order isogeometric theory. They extracted the governing equations of motion of sandwich nanoplates by the Hamilton principle and solved by the Newmark method. Dynamic instability behavior of graphene nanoplatelets-reinforced porous sandwich plates subjected to periodic in-plane compressive loads based on a four-variable refined quasi-3D plate theory were investigated by Nguyen and Phan [26]. They used Bolotin's method to solve the Mathieu–Hill equation. Their results show that the thickness stretching effect should be carefully evaluated for moderate to thick plate structures, such as sandwich plates. Free vibration and buckling analyses of piezoelectric–piezomagnetic FG microplates in thermal environment using MSGT were investigated by Hung et al. [27]. They derived the equilibrium equations by using Hamilton's principle. They reported the effect of the electric voltage, power index, magnetic potential, length scale parameters and geometrical parameter on the dimensionless frequencies and critical buckling loads of microplates. Jin [28] used a refined plate theory to examine Interlaminar stress analysis of composite laminated plates reinforced with FG graphene particle. Tharwan et al. [29] utilized a novel refined three-variable quasi-3D shear deformation theory to study the buckling behavior of multi-directional FG curved nanobeam rested on elastic foundation. They used a novel solution to effectively address a range of boundary conditions. Quasi 3D free vibration and buckling analysis of non-uniform thickness sandwich porous plates in a hygro-thermal environment utilizing a refined plate theory and novel finite element model were provided by Hai Van and Hong [30]. They considered the non-uniform thickness sandwich porous plates as bi-directional FGM. Their results reveal that the novel porosity patterns and the boundary conditions have a substantial impact on the mechanical behaviors sandwich porous plates. Shahmohammadi et al. [31] extended the modified nonlocal FSDT to study buckling analysis of multilayered composite plates reinforced with FG carbon nanotube or FG graphene platelets resting on elastic foundation. A novel quasi-3D hyperbolic HSDT in association with nonlocal MSGD was considered by Ghandourah et al. [32] to analyze bending and buckling behaviors of FG graphene-reinforced nanocomposite plates. The modified model of Halpin–Tsai and the rule of mixture were employed to compute the effective young's modulus, Poisson's ratio and mass density of FG graphene-reinforced nanocomposite plates. The inclusion of thickness stretching, nonlocal parameter and the length-scale parameter has a significant effect on the response of the GRNC plate. Hung et al. [33] employed a quasi-3D HSDT to study bending response of FG saturated porous nanoplate resting on elastic foundation. According to their findings, the deflection and stresses increase by increasing the values of the nonlocal parameter. Daikh et al. [34] proposed a Quasi-3D HSDT to examine the buckling behavior of bilayer FG porous plates based on nonlocal strain gradient theory (NSGT). They developed the equilibrium equations using the virtual work principle and solved utilizing the Galerkin method to cover various boundary conditions. Shahzad et al. [35] analyzed the size-dependent nonlinear dynamic of piezoelectric nanobeam subjected to a time-dependent mechanical uniform load. They formulated the NSGT based on a quasi-3D beam theory to take into account the size dependency.

Sandwich structures are one of the most advanced and modern structures that are utilized for strengthening based on the materials used in their construction. Fixed and mobile refrigerated warehouses, metal industries, spatial structures, industrial and semi-industrial cold stores are examples of the use of sandwich structures in different industries. Piezoelectric materials have been widely employed as sensors and actuators in microelectromechanical systems (MEMS) and nanoelectromechanical systems (NEMS). In addition, various piezoelectric materials have been considered for applications in energy harvesting, biomedical engineering, and additive manufacturing.

Therefore, due to the existence of piezoelectric layers, piezoelectric nano-sandwiches have many applications in the medical industries including drug delivery, cartilage, nerve, skin, tendon and muscle regeneration and as well as military industrials.

Many researchers have investigated behavior of structures over the past centuries. Today, based on the growth and development of industries and the increasing progress of technology, it is necessary to achieve accurate and reliable results using new models and methods. The use of piezoelectric face sheets as sensors and actuators as well as protection and prevention of damage to FGMs is of great importance considering the cost of construction and the production process of these materials. According to the comprehensive mentioned literature survey and to the best of the authors' knowledge, there has been no attempt in relation to the study of the bi-axial buckling analysis of FG nano-plate covered with piezoelectric face-sheets by considering elastic foundations. Motivated by these considerations, the current paper is the first attempt in present the exact solution for size dependent quasi-3D buckling analysis of a three-layer FG nanoplate integrated with piezoelectric layers supported by orthotropic Pasternak medium subjected to electric field and in-plane forces. Surface effect responsible for size-dependent characteristics can become distinctly important for piezoelectric nanomaterials in which large surface-to-volume ratio. Also, understanding the buckling behavior of sandwich nano-systems could be a key point for the application in electromechanical resonators, hence, for the first time surface effect, neutral surface position of FGMs and thickness stretching effects together with NSGT are applied to sandwich piezoelectric nanoplate. Eventually, one of the innovations of the presented research is the presentation of comparative results in different models for the critical buckling load of the nano-plate.

2 MATHEMATICAL MODELING

2.1 Non-local strain gradient theory

The used assumptions and modifications are presented as following. In order to simulate the behavior of the structure and also to be close to the reality of the behavior of the material, the equations are considered based on the quasi-three-dimensional theory. The proposed theory has assumed higher order variations of transverse displacement along the thickness direction. In general, it is assumed that σ_3 is small compared to τ_{13} and τ_{23}, except in the shell edges, so that the hypothesis is a good approximation of the actual behavior of thick plates. The sheets are assumed to be ideally attached to the core, such that there is complete continuity between the layers and they are considered integral. No slip condition existed between the core and face sheets it is assumed. The FGM is modeled as a linear elastic material in the pre-yield condition.

In order to study of the size-dependent behavior of structures, the NSGT for solids is used. On the basis of the NSGT, the constitutive relations of this theory include the effects of nonlocal elastic stress field and strain gradient stress field. It is assumed that the components of stress and electric displacement can be stated in the following form [36-38]:

$$\sigma_{ij} = {\sigma^{(0)}}_{ij} - \nabla {\sigma^{(1)}}_{ij} \tag{1}$$

$$D_i = {D^{(0)}}_i - \nabla {D^{(1)}}_i \tag{2}$$

In these equations the classical and higher-order stresses are ${\sigma^{(0)}}_{ij}, {\sigma^{(1)}}_{ij}$ as well as the classical and higher-order electric displacements are ${D^{(0)}}_i, {D^{(1)}}_i$ that are related to strain and strain gradient $\varepsilon_{ij}, \varepsilon_{ij,j}$, respectively. Mathematically, ignoring the effect of body force, the general constitutive relations of NSGT incorporated with both non-locality and SGT for the homogeneous piezoelectric material can be simplified as follows [39]:

$$(1-\mu^2\nabla^2)\sigma_{ij} = (1-\ell^2\nabla^2){\sigma^{(1)}}_{ij} \tag{3}$$

$$(1-\mu^2\nabla^2)D_i = (1-\ell^2\nabla^2){D^{(1)}}_i \tag{4}$$

$$\nabla^2 = \partial^2/\partial x^2 + \partial^2/\partial y^2 \tag{5}$$

These parameters denote the size effect on the behaviors of Nano-scale structures. The 3D constitutive equation of piezoelectric face-sheets based on the non-local MSGT can be defined as [38-42]:

$$(1-\mu^2\nabla^2)\{\sigma_{ij}\}=(1-\ell^2\nabla^2)\{C_{ijkl}\varepsilon_{kl}-e_{kij}E_k\} \tag{6}$$

$$(1-\mu^2\nabla^2)\{D_i\}=(1-\ell^2\nabla^2)\{e_{ikl}\varepsilon_{kl}+\kappa_{kij}E_k\} \tag{7}$$

In which C_{ijkl} ,e_{kij} and κ_{kij} are the stiffness, piezoelectric and dielectric coefficients for the piezoelectric Nano-plate, respectively. Also E_k are the components of electric field which can be defined in terms of electric potential as follow [40-41]:

$$\{E_x \quad E_y \quad E_z\}=-\left\{\frac{\partial}{\partial x} \quad \frac{\partial}{\partial y} \quad \frac{\partial}{\partial \tilde{z}}\right\}\Phi(x,y,z,t) \tag{8}$$

$$\Phi(x,y,z,t)=2(\tilde{z}V_0/h_p)-\cos(\pi\tilde{z}/h_p)\phi(x,y,t) \tag{9}$$

In Eq. (9) V_0 is applied external electric voltage between top and bottom of piezoelectric layers. Also $\phi(x,y,t)$ represents the spatial variation of the electric potential in two-dimensional directions. The converted coordinate for upper and lower layers according to middle of piezoelectric face-sheets are assumed $\tilde{z}=z-(h_c/2)-(h_p/2)$ and $\tilde{z}=z+(h_c/2)+(h_p/2)$, respectively.

2.2 Surface piezoelectricity effects

In nano-scale structures, the surface or near-surface atoms are usually exposed to various environmental influences from their bulk counterparts. Factually, the fraction of energy stored in surface layers are significant compared with those stored in the bulk of the element. Indeed, one of the main features of nanostructures is high ratio between their surface and volume. Therefore, the surface elasticity is mixed with the non-classical continuum theories to investigate these important effects. The primary relations of stresses and electric displacements for the surface of the piezoelectric materials considering NSGT can be presented as [40-42]:

$$(1-\mu^2\nabla^2)\{\sigma_{sij}\}=(1-\ell^2\nabla^2)\{C_{sijkl}\varepsilon_{kl}-e_{skij}E_k+\tau_s\aleph\} \tag{10}$$

$$(1-\mu^2\nabla^2)\{D_i\}=(1-\ell^2\nabla^2)\{e_{sikl}\varepsilon_{kl}+\kappa_{skij}E_k\} \tag{11}$$

C_{sij} ,e_{sij} ,κ_{sij} and τ_s are the surface elastic constants, surface piezoelectric constants, surface dielectric constants and the residual surface stress tensor. Surface and residual stress effects are considered only at the upper and lower surfaces of the piezoelectric face-sheets. Also, $\aleph=\{\partial(w_s+w_b)/\partial y\ ,\partial(w_s+w_b)/\partial x\}$.

2.3 FG properties

The concerned FG Nano-plate is compound of ceramic and metal that the volume fractions of material and the effective properties of are continuously considered to be variable in the thickness direction. Neutral axis of FG materials is not coinciding with its mid-plane due to asymmetry of material properties in these materials. For this reason, by choosing a suitable origin of the coordinates in the direction of changes, the stretching and bending coupling is eliminated and investigation of FG plate behavior can easily be done since the properties are symmetric around it.

Here, z_{ms} and z_{ns} are specify the distance the middle surface and neutral surface of FG nano-plate, respectively as illustrated in Fig. 1. $()_C$ and $()_M$ are the subscripts that refer to ceramic and metal and also k is the gradient index that is attributed to the change in volume fraction of the material composition [43-46].

$$V_C = \left(\frac{1}{2} + \frac{z_{ms}}{h_c}\right)^k = \left(\frac{1}{2} + \frac{z_{ns} + z_0}{h_c}\right)^k \tag{12}$$

$$P(z) = (P_C - P_M)\left(\frac{1}{2} + \frac{z_{ns} + z_0}{h_c}\right)^k + P_M \tag{13}$$

$$z_0 = \left(\int_{-h_c/2}^{h_c/2} E(z_{ms}) z_{ms} dz_{ms}\right) \Big/ \left(\int_{-h_c/2}^{h_c/2} E(z_{ms}) dz_{ms}\right) \tag{3}$$

The parameter z_0 is the distance of neutral surface from the middle surface. The position of the neutral surface of the FG plate is specified to satisfy the first moment with respect to young's modulus [43]. It is necessary to mention that the material properties in the top $z = (h_c/2) - z_0$ and the bottom surfaces $z = -(h_c/2) - z_0$ of the FG plate are pure ceramic and pure metal, respectively. The computation of nonzero elastic constant C_{cij} by considering the thickness stretching can be introduced as [44]:

$$(1 - \mu^2\nabla^2)\{\sigma_{ij}\} = (1 - \ell^2\nabla^2)[C_{cijkl}]\{\varepsilon_{kl}\} \tag{15}$$

$$\begin{aligned} C_{c11} &= C_{c22} = C_{c33} = \frac{(1-\upsilon)E}{(1-2\upsilon)(1+\upsilon)} \\ C_{c12} &= C_{c13} = C_{c23} = \frac{\upsilon E}{(1-2\upsilon)(1+\upsilon)} \\ C_{c44} &= C_{c55} = C_{c66} = \frac{E}{2(1+\upsilon)} \end{aligned} \tag{46}$$

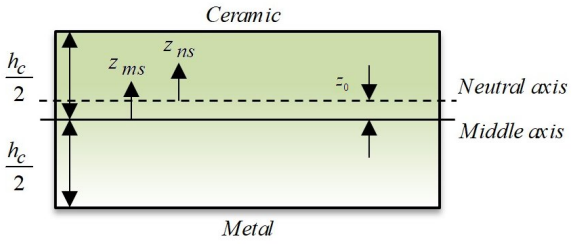

Fig. 1
Neutral surface position of FG nano-plate.

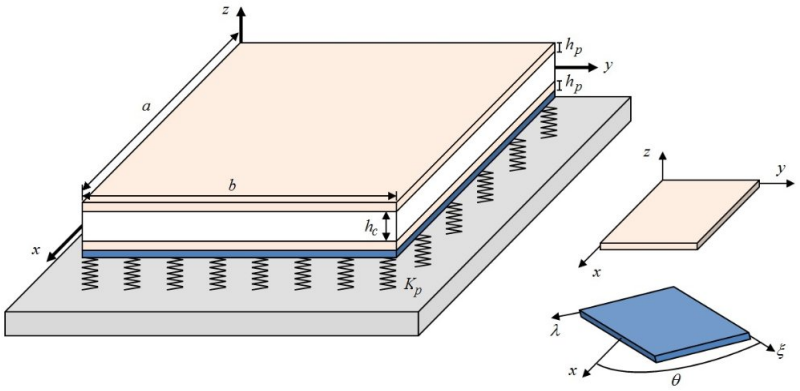

Fig. 2
Geometry of three-layered FG nano-plate integrated with piezoelectric face-sheets.

2.4 Displacement Field and Strains

The geometry and dimensions of a rectangular sandwich nano-plate of length a and width b is assumed as illustrated in Fig. 2. This sandwich structure is made of a FG base layer and piezoelectric face-sheets in top and bottom of core. The thickness of core and bonded layers are h_c and h_p, respectively. In this research a quasi-3D deformations plate theory based on the assumptions of the refined plate theory is used. The four-variable plate theory is developed by considering the thickness stretching. Consequently, the considered displacement field satisfies the conditions of transverse shear stresses in conjunction with shear strains at on the top and bottom surfaces of the sandwich plate. Accordingly, the orthogonal components of the displacement field can be defined as below [35,48];

$$u(x,y,z_{ns},t)=u_0-z_{ns}\frac{\partial w_b}{\partial x}-f(z_{ns})\frac{\partial w_s}{\partial x} \tag{17}$$

$$v(x,y,z_{ns},t)=v_0-z_{ns}\frac{\partial w_b}{\partial y}-f(z_{ns})\frac{\partial w_s}{\partial y} \tag{58}$$

$$w(x,y,z_{ns},t)=w_b+w_s+g(z_{ns})\varphi(x,y,t) \tag{6}$$

where u and v are the bending and shear components of mid-plane surface as well as w_b and w_s describe the unknown displacement functions of deflection, respectively. In these equations $f(z_{ns})$ is the transverse shear function in order to illustrate the transverse shear stresses and strains through the thickness. The shape functions can be expanded from the trigonometric, polynomial, hyperbolic functions and so on. In this study, the polynomial function is adopted as in the hybrid type quasi-3D shear deformation theory. The shape functions $f(z_{ns})$ and $g(z_{ns})$ can be expressed as [26,49];

$$f(z_{ns})=z_{ns}\left[-\frac{1}{4}+\frac{5}{3}\left(\frac{z_{ns}+z_0}{h}\right)^2\right] \tag{20}$$

$$g(z_{ns})=1-f'(z_{ns}) \tag{7}$$

The linear kinematic relations according to the displacement field can be written as follows:

$$\begin{Bmatrix}\varepsilon_{xx}\\ \varepsilon_{yy}\\ \gamma_{xy}\end{Bmatrix}=\begin{Bmatrix}\varepsilon^0_{xx}\\ \varepsilon^0_{yy}\\ \gamma^0_{xy}\end{Bmatrix}+z_{ns}\begin{Bmatrix}\kappa_x\\ \kappa_y\\ \kappa_{xy}\end{Bmatrix}+f\left(z_{ns}\right)\begin{Bmatrix}\eta_x\\ \eta_y\\ \eta_{xy}\end{Bmatrix},\qquad \begin{Bmatrix}\gamma_{xz}\\ \gamma_{yz}\end{Bmatrix}=g\left(z_{ns}\right)\begin{Bmatrix}\gamma^0_{xz}\\ \gamma^0_{yz}\end{Bmatrix},\qquad \varepsilon_{zz}=g'\left(z_{ns}\right)\varphi \tag{22}$$

where

$$\begin{Bmatrix}\varepsilon^0_{xx}\\ \varepsilon^0_{yy}\\ \gamma^0_{xy}\end{Bmatrix}=\begin{Bmatrix}\dfrac{\partial u_0}{\partial x}\\ \dfrac{\partial v_0}{\partial y}\\ \dfrac{\partial v_0}{\partial x}+\dfrac{\partial u_0}{\partial y}\end{Bmatrix},\quad \begin{Bmatrix}\kappa_x\\ \kappa_y\\ \kappa_{xy}\end{Bmatrix}=-\begin{Bmatrix}\dfrac{\partial^2 w_b}{\partial x^2}\\ \dfrac{\partial^2 w_b}{\partial y^2}\\ 2\dfrac{\partial^2 w_b}{\partial y\,\partial x}\end{Bmatrix}$$

$$\begin{Bmatrix}\eta_x\\ \eta_y\\ \eta_{xy}\end{Bmatrix}=-\begin{Bmatrix}\dfrac{\partial^2 w_s}{\partial x^2}\\ \dfrac{\partial^2 w_s}{\partial y^2}\\ 2\dfrac{\partial^2 w_s}{\partial y\,\partial x}\end{Bmatrix},\quad \begin{Bmatrix}\gamma^0_{xz}\\ \gamma^0_{yz}\end{Bmatrix}=\begin{Bmatrix}\dfrac{\partial w_s}{\partial x}+\dfrac{\partial \varphi}{\partial x}\\ \dfrac{\partial w_s}{\partial y}+\dfrac{\partial \varphi}{\partial y}\end{Bmatrix} \tag{23}$$

2.5 Equations of motion

Hamilton's principle is applied herein for deriving the equilibrium equations of the size-dependent sandwich nano-plate. This principle can be described in analytical form as [50-53,59];

$$\int_0^t\left(\delta U-\delta W\right)dt=0 \tag{24}$$

The variation of strain energy and the virtual work done by external applied forces and foundation can be expressed by δU and δW . The sandwich nano-plate is resting on the orthotropic Pasternak foundation. Contrary to other models, this foundation models both normal and shear loads in arbitrary directions. The applied force from the elastic foundation is calculated according to the orthotropic Pasternak model as [51,54-57]:

$$\delta W=\iint\left(\bar{N}-\bar{F}\right)\delta w\,dA \tag{25}$$

$$\bar{N}=\left\{\overline{N}_{xx}\quad \overline{N}_{yy}\right\}\left(\frac{\partial^2}{\partial x^2}+\frac{\partial^2}{\partial y^2}\right)\left(w_b+w_s\right) \tag{26}$$

$$\bar{F}=K_w w-K_{gx}\left(\cos^2\theta\frac{\partial^2 w}{\partial x^2}+\sin 2\theta\frac{\partial^2 w}{\partial x\,\partial y}+\sin^2\theta\frac{\partial^2 w}{\partial y^2}\right)-K_{gy}\left(\sin^2\theta\frac{\partial^2 w}{\partial x^2}-\sin 2\theta\frac{\partial^2 w}{\partial x\,\partial y}+\cos^2\theta\frac{\partial^2 w}{\partial y^2}\right) \tag{8}$$

In Eq. (26) longitudinal ($\bar{N}_{xx}$) and transverse ($\bar{N}_{yy}$) resultant are $N_{xx}+N_{ex}$ and $N_{yy}+N_{ey}$, respectively. The variations of total potential energy of the rectangular sandwich nano-plate consist of a FG core integrated with piezoelectric face-sheets can be expressed as

$$\begin{aligned}\delta U = &\iiint\left(\sigma_{xx}^{b}\delta\varepsilon_{xx}+\sigma_{yy}^{b}\delta\varepsilon_{yy}+\sigma_{zz}^{b}\delta\varepsilon_{zz}+\sigma_{xy}^{b}\delta\gamma_{xy}+\sigma_{xz}^{b}\delta\gamma_{xz}+\sigma_{yz}^{b}\delta\gamma_{yz}-D_{x}^{b}\delta E_{x}-D_{y}^{b}\delta E_{y}-D_{z}^{b}\delta E_{z}\right)dV\\ &+\iint\left(\sigma_{xx}^{s}\delta\varepsilon_{xx}+\sigma_{yy}^{s}\delta\varepsilon_{yy}+\sigma_{zz}^{s}\delta\varepsilon_{zz}+\sigma_{xy}^{s}\delta\gamma_{xy}+\sigma_{xz}^{s}\delta\gamma_{xz}+\sigma_{yz}^{s}\delta\gamma_{yz}-D_{x}^{s}\delta E_{x}-D_{y}^{s}\delta E_{y}-D_{z}^{s}\delta E_{z}\right)dA\Big|_{z_1}\\ &+\iint\left(\sigma_{xx}^{s}\delta\varepsilon_{xx}+\sigma_{yy}^{s}\delta\varepsilon_{yy}+\sigma_{zz}^{s}\delta\varepsilon_{zz}+\sigma_{xy}^{s}\delta\gamma_{xy}+\sigma_{xz}^{s}\delta\gamma_{xz}+\sigma_{yz}^{s}\delta\gamma_{yz}-D_{x}^{s}\delta E_{x}-D_{y}^{s}\delta E_{y}-D_{z}^{s}\delta E_{z}\right)dA\Big|_{z_2}\end{aligned} \tag{9}$$

$$\delta U=\iint\begin{pmatrix}-\dfrac{\partial(N_{x}^{b}+N_{x}^{s})}{\partial x}\delta u-\dfrac{\partial(N_{xy}^{b}+N_{xy}^{s})}{\partial y}\delta u-2\dfrac{\partial^{2}(M_{sxy}^{b}+M_{sxy}^{s})}{\partial x\,\partial y}\delta w_{s}-\dfrac{\partial^{2}(M_{by}^{b}+M_{by}^{s})}{\partial y^{2}}\delta w_{b}\\ -\dfrac{\partial^{2}(M_{bx}^{b}+M_{bx}^{s})}{\partial x^{2}}\delta w_{b}-\dfrac{\partial(N_{xy}^{b}+N_{xy}^{s})}{\partial x}\delta v-\dfrac{\partial(N_{y}^{b}+N_{y}^{s})}{\partial y}\delta v-\dfrac{\partial^{2}(M_{sx}^{b}+M_{sx}^{s})}{\partial x^{2}}\delta w_{s}\\ -\dfrac{\partial^{2}(M_{sy}^{b}+M_{sy}^{s})}{\partial y^{2}}\delta w_{s}+(N_{z}^{b}+N_{z}^{s})\delta\varphi-\left(\dfrac{\partial(Q_{yz}^{b}+Q_{yz}^{s})}{\partial y}+\dfrac{\partial(Q_{xz}^{b}+Q_{xz}^{s})}{\partial x}\right)\left[\delta w_{s}-\delta\varphi\right]\\ +\left(T_{x}^{b}+T_{x}^{s}+T_{y}^{b}+T_{y}^{s}+T_{z}^{b}+T_{z}^{s}\right)\delta\phi-2\dfrac{\partial^{2}(M_{bxy}^{b}+M_{bxy}^{s})}{\partial x\,\partial y}\delta w_{b}\end{pmatrix}dA \tag{10}$$

In the above equation, z_1 and z_2 are defined as $-(h_c/2)-h_p-z_0$ and $(h_c/2)+h_p-z_0$. Also, N, M and Q refers to the force, moment and transverse shear stress resultants that can be defined as:

$$\begin{bmatrix}N_{x}^{i} & M_{bx}^{i} & M_{sx}^{i}\\ N_{y}^{i} & M_{by}^{i} & M_{sy}^{i}\\ N_{xy}^{i} & M_{bxy}^{i} & M_{sxy}^{i}\end{bmatrix}=\sum_{r=1}^{3}\int_{h_r-z_0}^{h_{r+1}-z_0}\begin{pmatrix}1 & z_{ns} & f(z_{ns})\end{pmatrix}\begin{Bmatrix}\sigma_{xx}^{i}\\ \sigma_{yy}^{i}\\ \sigma_{xy}^{i}\end{Bmatrix}dz_{ns} \tag{30}$$

$$\begin{bmatrix}Q_{xz}^{i} & Q_{yz}^{i}\end{bmatrix}=\sum_{r=1}^{3}\int_{h_r-z_0}^{h_{r+1}-z_0}g(z_{ns})\begin{Bmatrix}\sigma_{xz}^{i} & \sigma_{yz}^{i}\end{Bmatrix}dz_{ns} \tag{31}$$

$$N_{z}^{i}=\sum_{r=1}^{3}\int_{h_r-z_0}^{h_{r+1}-z_0}g'(z_{ns})\left\{\sigma_{zz}^{i}\right\}dz_{ns} \tag{32}$$

$$\begin{Bmatrix}T_{x}^{i} & T_{y}^{i} & T_{z}^{i}\end{Bmatrix}=\sum_{r=1}^{3}\int_{h_r-z_0}^{h_{r+1}-z_0}\begin{bmatrix}\cos\left(\dfrac{\pi\bar{z}_{ns}}{h_p}\right)\dfrac{\partial D_{x}^{i}}{\partial x} & \cos\left(\dfrac{\pi\bar{z}_{ns}}{h_p}\right)\dfrac{\partial D_{y}^{i}}{\partial y} & \sin\left(\dfrac{\pi\bar{z}_{ns}}{h_p}\right)\dfrac{D_{z}^{i}\pi}{h_p}\end{bmatrix}dz_{ns} \tag{11}$$

where h_{r+1} and h_r are the top and the bottom of the $r-th$ layer, respectively. Also, the converted coordinate based on the neutral axis is $\bar{z}_{ns}=z_{ns}\pm(h_c/2)\pm(h_p/2)-z_0$. The bulk and surface coefficients can be obtained by substituting Eqs. (6)-(7) into Eqs. (30)-(33). Finally, based on the Hamilton's principles, integrating by parts and setting the coefficient of mechanical and electrical $(\delta u,\delta v,\delta w_b,\delta w_s,\delta\varphi,\delta\phi)$ to zero, separately, the non-local equilibrium equations of sandwich nano-plate resting on elastic foundation are derived for the refined plate theory as:

$$\delta u:(1-\ell^{2}\nabla^{2})\begin{Bmatrix}(A_{66}^{b}+A_{66}^{s})(\dfrac{\partial^{2}v}{\partial y\,\partial x}+\dfrac{\partial^{2}u}{\partial y^{2}})-(B_{11}^{b}+B_{11}^{s})\dfrac{\partial^{3}w_{b}}{\partial x^{3}}-(F_{11}^{b}+F_{11}^{s})\dfrac{\partial^{3}w_{s}}{\partial x^{3}}\\ -(B_{12}^{b}+B_{12}^{s})\dfrac{\partial^{3}w_{b}}{\partial y^{2}\partial x}-(F_{12}^{b}+F_{12}^{s})\dfrac{\partial^{3}w_{s}}{\partial y^{2}\partial x}+(A_{11}^{b}+A_{11}^{s})\dfrac{\partial^{2}u}{\partial x^{2}}+(A_{12}^{b}+A_{12}^{s})\dfrac{\partial^{2}v}{\partial y\,\partial x}\\ +(D_{11}^{b}+D_{11}^{s}+E_{11}^{b}+E_{11}^{s})\dfrac{\partial\phi}{\partial x}-2(B_{66}^{b}+B_{66}^{s})\dfrac{\partial^{3}w_{b}}{\partial y^{2}\partial x}-2(F_{66}^{b}+F_{66}^{s})\dfrac{\partial^{3}w_{s}}{\partial y^{2}\partial x}\end{Bmatrix} \tag{12}$$

$$\delta v:(1-\ell^2\nabla^2)\left\{\begin{array}{l}(A_{12}^b+A_{12}^s)\dfrac{\partial^2 u}{\partial y\,\partial x}-2(B_{66}^b+B_{66}^s)\dfrac{\partial^3 w_b}{\partial y\,\partial x^2}-(B_{11}^b+B_{11}^s)\dfrac{\partial^3 w_b}{\partial y^3}-(F_{11}^b+F_{11}^s)\dfrac{\partial^3 w_s}{\partial y^3}\\ +(A_{66}^b+A_{66}^s)(\dfrac{\partial^2 v}{\partial x^2}+\dfrac{\partial^2 u}{\partial y\,\partial x})-(B_{12}^b+B_{12}^s)\dfrac{\partial^3 w_b}{\partial y\,\partial x^2}-(F_{12}^b+F_{12}^s)\dfrac{\partial^3 w_s}{\partial y\,\partial x^2}\\ +(D_{11}^b+D_{11}^s+E_{11}^b+E_{11}^s)\dfrac{\partial\phi}{\partial y}-2(F_{66}^b+F_{66}^s)\dfrac{\partial^3 w_s}{\partial y\,\partial x^2}+(A_{11}^b+A_{11}^s)\dfrac{\partial^2 v}{\partial y^2}\end{array}\right\} \tag{13}$$

$$\delta w_b:(1-\mu^2\nabla^2)\{\bar{N}-\bar{F}\}+(1-\ell^2\nabla^2)\left\{\begin{array}{l}(B_{11}^b+B_{11}^s)(\dfrac{\partial^3 u}{\partial x^3}+\dfrac{\partial^3 v}{\partial y^3})+2(B_{66}^b+B_{66}^s)(\dfrac{\partial^3 v}{\partial y\,\partial x^2}+\dfrac{\partial^3 u}{\partial y^2\partial x})\\ -2(J_{12}^b+J_{12}^s)\dfrac{\partial^4 w_b}{\partial y^2\partial x^2}-(J_{11}^b+J_{11}^s)(\dfrac{\partial^4 w_b}{\partial x^4}+\dfrac{\partial^4 w_b}{\partial y^4})\\ -(R_{11}^b+R_{11}^s)(\dfrac{\partial^4 w_s}{\partial x^4}+\dfrac{\partial^4 w_s}{\partial y^4})-4(J_{66}^b+J_{66}^s)\dfrac{\partial^4 w_b}{\partial y^2\partial x^2}\\ +(D_{22}^b+D_{22}^s+E_{22}^b+E_{22}^s)(\dfrac{\partial^2\phi}{\partial x^2}+\dfrac{\partial^2\phi}{\partial y^2})+(B_{12}^b+B_{12}^s)(\dfrac{\partial^3 v}{\partial y\,\partial x^2}+\dfrac{\partial^3 u}{\partial y^2\partial x})\\ -2(R_{12}^b+R_{12}^s-2R_{66}^b-2R_{66}^s)\dfrac{\partial^4 w_s}{\partial y^2\partial x^2}\end{array}\right\} \tag{14}$$

$$\delta w_s:(1-\mu^2\nabla^2)\{\bar{N}-\bar{F}\}+(1-\ell^2\nabla^2)\left\{\begin{array}{l}2(F_{66}^b+F_{66}^s)(\dfrac{\partial^3 v}{\partial y\,\partial x^2}+\dfrac{\partial^3 u}{\partial y^2\partial x})-2(R_{12}^b+R_{12}^s)\dfrac{\partial^4 w_b}{\partial y^2\partial x^2}\\ -(R_{11}^b+R_{11}^s)(\dfrac{\partial^4 w_b}{\partial x^4}+\dfrac{\partial^4 w_b}{\partial y^4})-(L_{11}^b+L_{11}^s)(\dfrac{\partial^4 w_s}{\partial y^4}+\dfrac{\partial^4 w_s}{\partial x^4})\\ +P_{11}^s(\dfrac{\partial^2 w_b}{\partial y^2}+\dfrac{\partial^2 w_s}{\partial y^2})-2(L_{12}^b+L_{12}^s)\dfrac{\partial^4 w_s}{\partial y^2\partial x^2}-4(L_{66}^b+L_{66}^s)\dfrac{\partial^4 w_s}{\partial y^2\partial x^2}\\ +P_{11}^s(\dfrac{\partial^2 w_b}{\partial x^2}+\dfrac{\partial^2 w_s}{\partial x^2})-4(R_{66}^b+R_{66}^s)\dfrac{\partial^4 w_b}{\partial y^2\partial x^2}\\ +(D_{33}^b+D_{33}^s)(\dfrac{\partial^2\varphi}{\partial x^2}+\dfrac{\partial^2\varphi}{\partial y^2})-H_{11}^b(\dfrac{\partial^2\phi}{\partial x^2}-\dfrac{\partial^2\phi}{\partial y^2})\\ +(E_{33}^b+E_{33}^s)(\dfrac{\partial^2\phi}{\partial x^2}+\dfrac{\partial^2\phi}{\partial y^2})+(F_{12}^b+F_{12}^s)(\dfrac{\partial^3 v}{\partial y\,\partial x^2}+\dfrac{\partial^3 u}{\partial y^2\partial x})+\\ G_{11}^b(\dfrac{\partial^2\varphi}{\partial y^2}+\dfrac{\partial^2 w_s}{\partial y^2})+G_{22}^b(\dfrac{\partial^2\varphi}{\partial x^2}+\dfrac{\partial^2 w_s}{\partial x^2})+(F_{11}^b+F_{11}^s)(\dfrac{\partial^3 u}{\partial x^3}+\dfrac{\partial^3 v}{\partial y^3})\end{array}\right\} \tag{15}$$

$$\delta\varphi:\ (1-\ell^2\nabla^2)\left\{\begin{array}{l}(D_{22}^b+D_{22}^s)(\dfrac{\partial^2 w_b}{\partial x^2}+\dfrac{\partial^2 w_b}{\partial y^2})-(D_{11}^b+D_{11}^s)(\dfrac{\partial u}{\partial x}+\dfrac{\partial v}{\partial y})-H_{11}^b(\dfrac{\partial^2\phi}{\partial x^2}-\dfrac{\partial^2\phi}{\partial y^2})\\ +P_{11}^s(\dfrac{\partial^2 w_b}{\partial y^2}+\dfrac{\partial^2 w_s}{\partial y^2})+G_{11}^b(\dfrac{\partial^2\varphi}{\partial y^2}+\dfrac{\partial^2 w_s}{\partial y^2})+G_{22}^b(\dfrac{\partial^2\varphi}{\partial x^2}+\dfrac{\partial^2 w_s}{\partial x^2})\\ +P_{11}^s(\dfrac{\partial^2 w_b}{\partial x^2}+\dfrac{\partial^2 w_s}{\partial x^2})+(D_{33}^b+D_{33}^s)(\dfrac{\partial^2 w_s}{\partial x^2}+\dfrac{\partial^2 w_s}{\partial y^2})\end{array}\right\} \tag{16}$$

$$\delta\phi:\ (1-\ell^2\nabla^2)\begin{Bmatrix}(I_{11}^b+I_{11}^s)(\frac{\partial^2\phi}{\partial x^2}+\frac{\partial^2\phi}{\partial y^2})+(B_{33}^b+B_{33}^s)\varphi-(I_{33}^b+I_{33}^s)\phi\\-(E_{33}^b+E_{33}^s)(\frac{\partial^2 w_s}{\partial x^2}+\frac{\partial^2 w_s}{\partial y^2})+(E_{11}^b+E_{11}^s)(\frac{\partial u}{\partial x}+\frac{\partial v}{\partial y})\\-(E_{22}^b+E_{22}^s)(\frac{\partial^2 w_b}{\partial x^2}+\frac{\partial^2 w_b}{\partial y^2})+(H_{11}^b+H_{11}^s)(\frac{\partial^2\varphi}{\partial x^2}+\frac{\partial^2 w_s}{\partial x^2}+\frac{\partial^2\varphi}{\partial y^2}+\frac{\partial^2 w_s}{\partial y^2})\end{Bmatrix} \tag{17}$$

which the stiffness and piezoelectric coefficients for bulk and surface FG sandwich nano-plate after simplification are given by:

$$\begin{Bmatrix}A_{ij}^b & B_{ij}^b & J_{ij}^b\\F_{ij}^b & R_{ij}^b & L_{ij}^b\end{Bmatrix}=\sum_{r=1}^{3}\int_{h_r-z_0}^{h_{r+1}-z_0}C_{ij}^b\begin{Bmatrix}1 & z_{ns} & z_{ns}^2\\f(z_{ns}) & z_{ns}f(z_{ns}) & f^2(z_{ns})\end{Bmatrix}dz_{ns}\qquad i,j=1,2,6 \tag{4018}$$

$$\left\{D_{ii}^b,E_{ii}^b\right\}=\sum_{r=1}^{3}\int_{h_r-z_0}^{h_{r+1}-z_0}\left[C_{13}^b g'(z_{ns}),\frac{\pi}{h_p}e_{13}^b\sin\left(\frac{\pi\bar{z}_{ns}}{h_p}\right)\right]\{1,z_{ns},f(z_{ns})\}dz_{ns}\qquad i=1,2,3 \tag{41}$$

$$\left\{G_{11}^b,G_{22}^b\right\}=\sum_{r=1}^{3}\int_{h_r-z_0}^{h_{r+1}-z_0}\left[C_{44}^b,C_{55}^b\right]g^2(z_{ns})dz_{ns} \tag{42}$$

$$\left\{H_{11}^b,H_{22}^b\right\}=\sum_{r=1}^{3}\int_{h_r-z_0}^{h_{r+1}-z_0}\left[e_{15}^b,e_{24}^b\right]g(z_{ns})\cos\left(\frac{\pi\bar{z}_{ns}}{h_p}\right)dz_{ns} \tag{43}$$

$$\left\{I_{11}^b,I_{22}^b\right\}=\sum_{r=1}^{3}\int_{h_r-z_0}^{h_{r+1}-z_0}\left[\in_{11}^b,\in_{22}^b\right]\sin^2\left(\frac{\pi\bar{z}_{ns}}{h_p}\right)dz_{ns} \tag{44}$$

$$\left\{A_{33}^b,B_{33}^b,I_{33}^b\right\}=\sum_{r=1}^{3}\int_{h_r-z_0}^{h_{r+1}-z_0}\left[C_{33}^b g'^2(z_{ns}),\frac{\pi}{h_p}e_{33}^b g'(z_{ns})\sin\left(\frac{\pi\bar{z}_{ns}}{h_p}\right),\frac{\pi^2}{h_p^2}\in_{33}^b\sin^2\left(\frac{\pi\bar{z}_{ns}}{h_p}\right)\right]dz_{ns} \tag{45}$$

$$\begin{Bmatrix}A_{ij}^s & B_{ij}^s & J_{ij}^s\\F_{ij}^s & R_{ij}^s & L_{ij}^s\end{Bmatrix}=C_{ij}^s\begin{Bmatrix}1 & z_{ns} & z_{ns}^2\\f(z_{ns}) & z_{ns}f(z_{ns}) & f^2(z_{ns})\end{Bmatrix}\Bigg|_{z_{ns}=\pm\frac{h_c}{2}\pm h_p-z_0}\qquad i,j=1,2,6 \tag{46}$$

$$\left\{D_{ii}^s,E_{ii}^s\right\}=\left[C_{13}^s g'(z_{ns}),\frac{\pi}{h_p}e_{13}^s\sin\left(\frac{\pi\bar{z}_{ns}}{h_p}\right)\right]\{1,z_{ns},f(z_{ns})\}\Bigg|_{z_{ns}=\pm\frac{h_c}{2}\pm h_p-z_0}\qquad i=1,2,3 \tag{47}$$

$$\left\{I_{11}^s,I_{22}^s\right\}=\left[\in_{11}^s,\in_{22}^s\right]\sin^2\left(\frac{\pi\bar{z}_{ns}}{h_p}\right)\Bigg|_{z_{ns}=\pm\frac{h_c}{2}\pm h_p-z_0} \tag{48}$$

$$\left\{A_{33}^s,B_{33}^s,I_{33}^s\right\}=\left[C_{33}^s g'^2(z_{ns}),\frac{\pi}{h_p}e_{33}^s g'(z_{ns})\sin\left(\frac{\pi\bar{z}_{ns}}{h_p}\right),\frac{\pi^2}{h_p^2}\in_{33}^s\sin^2\left(\frac{\pi\bar{z}_{ns}}{h_p}\right)\right]\Bigg|_{z_{ns}=\pm\frac{h_c}{2}\pm h_p-z_0} \tag{48}$$

$$\left\{H_{11}^{s}\right\}=\left\{H_{22}^{s}\right\}=\left[e_{15}^{s}\, g\left(z_{ns}\right)\cos\left(\frac{\pi \bar{z}_{ns}}{h_p}\right)\right]\Bigg|_{z_{ns}=\pm\frac{h_c}{2}\pm h_p-z_0} \tag{50}$$

$$\left\{P_{11}^{s}\right\}=\left[\tau_s\, g\left(z_{ns}\right)\right]\Big|_{z_{ns}=\pm\frac{h_c}{2}\pm h_p-z_0} \tag{51}$$

3 SOLUTION PROCEDURE OF SIMPLY-SUPPORTED NANO-PLATE

The analytical method is employed in order to solve motion equations. Based on Navier's solution procedure, the expansions of displacement functions can be defined in space variables as [14];

$$\begin{aligned}
&u\left(x,y,t\right)=U_{mn}\cos\left(\alpha x\right)\sin\left(\beta y\right)\\
&v\left(x,y,t\right)=V_{mn}\sin\left(\alpha x\right)\cos\left(\beta y\right)\\
&w_b\left(x,y,t\right)=W_{bmn}\sin\left(\alpha x\right)\sin\left(\beta y\right)\\
&w_s\left(x,y,t\right)=W_{smn}\sin\left(\alpha x\right)\sin\left(\beta y\right)\\
&\varphi\left(x,y,t\right)=\Phi_{mn}\sin\left(\alpha x\right)\sin\left(\beta y\right)\\
&\phi\left(x,y,t\right)=\Theta_{mn}\sin\left(\alpha x\right)\sin\left(\beta y\right)
\end{aligned} \tag{52}$$

where $\{U_{mn},V_{mn},W_{bmn},W_{smn},\Phi_{mn},\Theta_{mn}\}$ are the unknown coefficients which should be determined. Also $\alpha=m\pi/a$ and $\beta=n\pi/b$ are constant coefficients related to the mode numbers (m,n) in x and y directions, respectively. By inserting Eq. (40) into Eqs. (34)-(39), buckling analysis of sandwich nano-plate with FG core and piezoelectric face-sheets subjected to a system of uniform in-plane compressive loads can be expressed as follow:

$$\left(\left[K\right]-\left[S\right]\right)\{\mathrm{X}_{mn}\}=0 \tag{53}$$

$$\det\left(\left[K\right]-\left[S\right]\right)=0 \tag{54}$$

in which $[K]$ and $[S]$ denote the stiffness and in-plane forces matrix's and also $\{\mathrm{X}_{mn}\}$ represents unknown coefficients $\{U_{mn},V_{mn},W_{bmn},W_{smn},\Phi_{mn},\Theta_{mn}\}$. In order to obtain the critical buckling load for various kinds of boundary conditions, it is necessary to calculate the determinant of the coefficient matrix in Eq. (41) and set it equal to zero. The critical buckling load is the smallest value of N_0.

4 NUMERICAL RESULTD AND DISCUSSION

In the numerical results, bi-axial buckling behavior of FG nano-plate covered with piezoelectric face-sheets is presented based on the surface piezoelasticity theory. The FG nano-plate in the following examples is assumed to be made up of metal (aluminum) and ceramic (alumina) which the material properties are as follows: $E_m=70GPa, E_c=380GPa, \upsilon=0.3$ [50]. On the other hand, piezoelectric face-sheets are supposed to be composed of ZnO which its bulk and surface properties are used based on Ghorbanpour Arani et al. [56]. The common values are chosen to carry out the following analyses.

$$\begin{aligned}
&\mu=\ell=1(nm), V_0=-5(v), k=1, a/b=2, h=3(nm), \tau_s=1(N/m), m=n=1,\\
&K_w=1\text{^}17(N/m^3), \theta=\pi/4, K_{gx}=10(N/m), K_{gy}=20(N/m), h_c/h_p=10
\end{aligned}$$

Table 1
Comparison of buckling load of FG plate for various power-law index

P	Model	Axial/Bi-axial	Non-dimensional critical buckling load					
			1-0-1	2-1-2	2-1-1	1-1-1	2-2-1	1-2-1
0	El Meiche et al. [50]	Axial	13.00552	13.00552	13.00552	13.00552	13.00552	13.00552
	Present Model		13.00552	13.00552	13.12398	13.00552	13.07977	13.00552
	El Meiche et al. [50]	Bi-axial	6.50276	6.50276	6.50276	6.50276	6.50276	6.50276
	Present Model		6.50326	6.50425	6.56199	6.50276	6.53988	6.50280
1	El Meiche et al. [50]	Axial	5.16629	5.83941	6.19371	6.46450	6.94952	7.50719
	Present Model		5.16712	5.84012	6.21936	6.46750	6.96728	7.50991
	El Meiche et al. [50]	Bi-axial	2.58315	2.91970	3.09686	3.23225	3.47476	3.75359
	Present Model		2.58317	2.92010	3.10968	3.23245	3.48364	3.75652
5	El Meiche et al. [50]	Axial	2.65679	3.04141	3.40280	3.57873	4.11157	4.73463
	Present Model		2.65600	3.04527	3.41752	3.57900	4.12120	4.73785
	El Meiche et al. [50]	Bi-axial	1.32839	1.52071	1.70140	1.78937	2.05578	2.36731
	Present Model		1.32840	1.52070	1.70876	1.79136	2.06060	2.37011
10	El Meiche et al. [50]	Axial	2.48574	2.74498	3.09111	3.19373	3.70686	4.27964
	Present Model		2.48998	2.74652	3.10632	3.19993	3.71037	4.28215
	El Meiche et al. [50]	Bi-axial	1.24287	1.37249	1.54556	1.59687	1.85343	2.13982
	Present Model		1.24381	1.37989	1.55316	1.60120	1.85915	2.14001

At this stage, it is necessary to provide a comprehensive comparison in order to validity and accuracy of the used model. Therefore, a comparison study of axial and bi-axial critical buckling loads of FG sandwich plate is presented in Fig. 3. In addition, the accuracy of the presented plate theory and appropriateness of solution approach are assessed by simulating the response the dimensionless buckling load of sandwich plate with different thickness ratio as shown in Table 1 [50]. It is observed from Table 1 and Fig. 3 that the numerical results have excellent agreements with the obtained results in available references [50]. On the other hand, comparison of nondimensional critical buckling load of isotropic plate under different loading types are in Table 2. In this Table, the results based on the FSDT, TSDT and sinusoidal shear deformation theories with the present model have been examined according to length to width ratio as well as thickness to width ratio. Table 2 shows that in different loading conditions, there is a good agreement between the existing results and the investigated model.

The size-dependent behavior of FG nano-plate based on material characteristic and non-local parameter is demonstrated in Fig. 4. As can be observed nonlocal and length scale parameters have a stiffness-softening influence on behavior of FG nano-plate structure. The critical buckling load of FG nano-plate is reduced by applying non-local theory. On the other hand, inclusion of length scale parameter leads to increasing in critical buckling load of FG nano-plate, especially in the lower non-locality parameter. In addition, the effect of the softening enhancement of sandwich nanostructure is applied by considering NSGT. Increasing the nonlocal parameter result in a decrease in the stiffness of the sandwich nano plate and therefore its critical buckling load decreases. The length scale parameter, as a fundamental factor, plays an important role in approximating the critical load values of nanostructures. As mentioned in the mathematical modeling section, in this research, this parameter is applied using NSGT. Increasing this parameter increases the stiffness of the structure and also increases the critical load, which results in an increase in the static stability of the structure.

Table 2
Comparison of nondimensional critical buckling load of isotropic plate under different loading types

a/b	h/b	Method	Loading type (γ_1, γ_2)		
			(-1,0)	(0, -1)	(-1, -1)
1	0.1	FSDT [58]	3.7865	3.7865	1.8932
		TSDT [58]	3.7866	3.7866	1.8933
		SSDT [57]	3.7869	3.7869	1.8935
		Present	3.7875	3.7881	1.8952
	0.2	FSDT [58]	3.2637	3.2637	1.6319
		TSDT [58]	3.2653	3.2653	1.6327
		SSDT [57]	3.2666	3.2666	1.6333
		Present	3.2684	3.2692	1.636
1.5	0.1	FSDT [58]	4.025	2.0048	1.3879
		TSDT [58]	4.0253	2.0048	1.3879
		SSDT [57]	4.0258	2.0049	1.388
		Present	4.0274	2.0082	1.4006
	0.2	FSDT [58]	3.3048	1.7941	1.2421
		TSDT [58]	3.3077	1.7946	1.2424
		SSDT [57]	3.3096	1.7951	1.2427
		Present	3.3123	1.7973	1.2461
2	0.1	FSDT [58]	3.7865	1.5093	1.2074
		TSDT [58]	3.7866	1.5093	1.2075
		SSDT [57]	3.7869	1.5094	1.2075
		Present	3.7875	1.5108	1.2084
	0.2	FSDT [58]	3.2637	1.3694	1.0955
		TSDT [58]	3.2654	1.3697	1.0958
		SSDT [57]	3.2666	1.37	1.096
		Present	3.2684	1.3726	1.0987

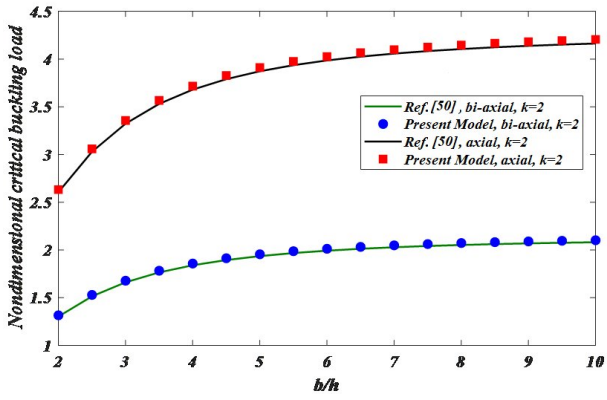

Fig. 3
Comparison present results with those obtained by El Meiche et al. [50].

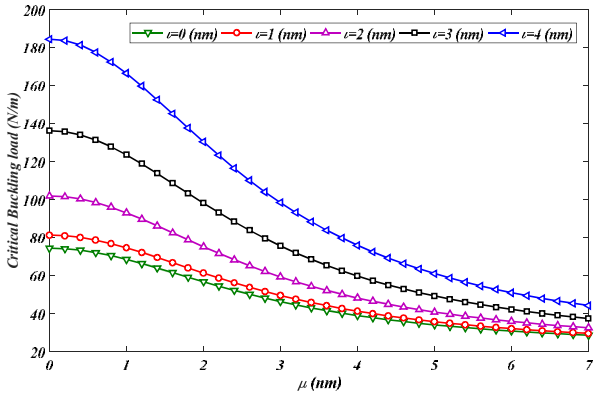

Fig. 4
Effects of length scale parameter on the buckling load for various non-local parameter.

The variations of bi-axial buckling response versus electrical preload for face-sheets subjected to an electric potential are investigated in Fig. 5. According to this figure, the positive and negative electrical preloads are as tensile and compressive loads. The application of tensile and compressive preloads caused by external voltage leads to the creation of prestresses in the structure. By applying a negative voltage load, the stiffness increases and the static stability of the structure improves, and considering the positive initial voltage, the stiffness decreases and as a result, the critical load of the structure decreases. The changes of critical buckling load with increasing the initial voltage from -5 to 5 volt, for different power-law index, is equal 9.54%, 13.7%, 14.78%, 15.66% and 16.31%, respectively. Also, Fig. 5 shows an increase in the power-law index, which leads to an increase/decrease in metallic/ceramic properties along the thickness of the structure. Due to the lower elastic modulus and as a result the stiffness of the metal material compared to the ceramic material, the rigidity of the core is reduced and as a result the critical load of the structure is reduced.

Fig. 6 examines the influences the external electric voltage and the thicknesses ratio on critical buckling load of non-local nano-plate under electrical field. The critical load decrease with the increasing value of the thicknesses of face-sheets. According to the material considered for the FG core, increasing the thickness of the core compared to the total thickness leads to a reduction in the stiffness of the structure and a reduction in the critical load. The results reveal that the effect of reducing buckling load in lower values of h_p/h is more noticeable.

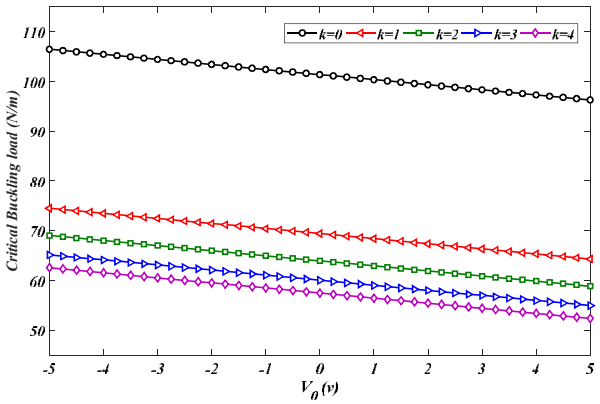

Fig. 5
Influence of gradient index on the critical load with respect to various initial voltage.

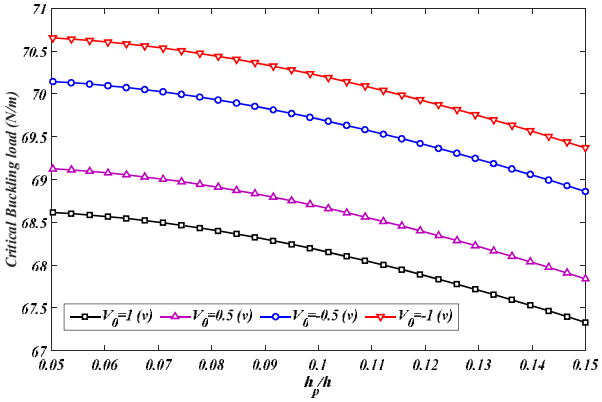

Fig. 6
Variation of buckling response with respect to various thicknesses ratio.

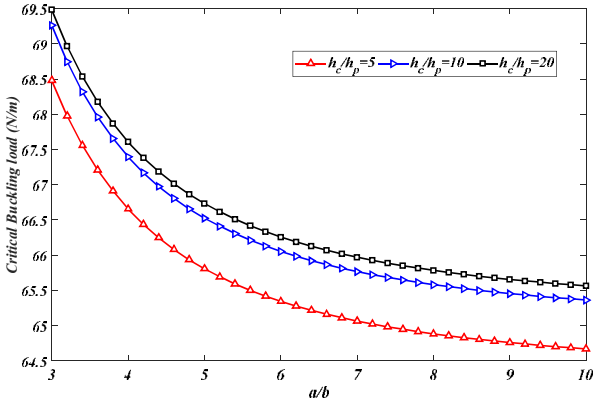

Fig. 7
Critical buckling load versus aspect ratio for various core-to-face-sheets thicknesses ratio.

In Fig. 7 shows buckling results of FG nano-plate various the core-to-face-sheets thickness and length-to-width ratios, simultaneously. It can be seen that by constant consideration of the total thickness and the core nonhomogeneous parameter, increasing thickness of core means a reduction at the thickness of piezoelectric layer. Since the stiffness of the core is higher than piezoelectric face-sheets, the increase in the thickness of the core leads to the improvement of the stiffness of the whole structure, and as a result, the critical load increases. On the other hand, the increase in the length-to-width ratio of nano-plate has an extraordinary efficacy on reduction the stiffness of the nano-plate, which decreases the buckling load. Increasing the length of the structure compared to its width, in general, changes the shape of the structure and ultimately changes the behavior of the nano-sandwich plate. Since with the increase of the length-to-width ratio of the nano-plate, the state of the structure tends to the beam model, finally in this state, the change of the buckling behavior is decreasing.

The effect of applying neutral axis on critical buckling load behavior of FG nano-plate coupled with piezoelectric face-sheets is depicted in Fig. 8 versus power-law-index and core's thickness. The employment of the neutral axis causes to a symmetrical arrangement of material properties in the thickness direction and consequently, the critical buckling load is reducing. It is clearly evident that the consideration of neutral axis is more noticeable at higher thicknesses. Both parameters of nonhomogeneous factor and core thickness are very effective in calculating the location of the neutral surface of FGM. It should be noted that the power-law index is more effective at higher thicknesses.

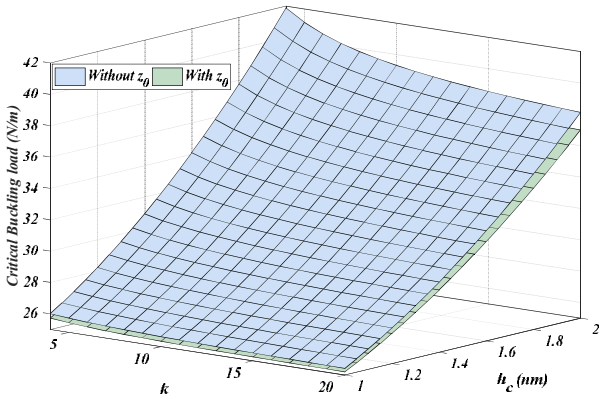

Fig. 8
buckling load versus power-law index and core's thickness with and without neutral surface.

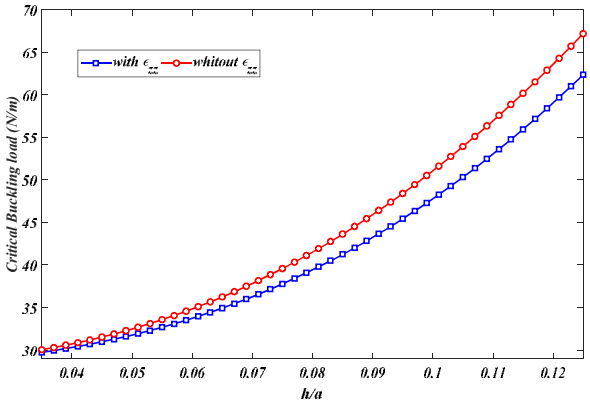

Fig. 9
Response of buckling load versus thickness-to-length ratio with and without stretching effect.

Fig. 9 presents the effect of stretching parameter on critical load of non-local FG nano-plates. Also, the effect of thickness-to-length ratio is examined. It can understand from this figure that the critical buckling load is reduced by considering the stretching effect. As can be seen, the predicted results of present quasi-3D and 2D models are almost the same at low thickness-to-length ratios and with the increase of this ratio, the difference between quasi-3D and 2D models increases greatly. Considering the parameters related to the relationships of the quasi-3D model shows results closer to reality and as Fig. 9 shows, the critical load in this case is lower than the two-dimensional case. This shows the omission of some parameters and the simplification of the equations in the 2D model, which has led to the calculation of a higher critical load. It can be concluded that the stretching effect is directly related to the thickness. As the thickness increases, the efficacy of the stretching is also increased. Fig. 10 illustrates the size-dependent behavior of nano-sized plate by considering surface elastic based on non-local and scale material parameters. It can be seen that when the non-local parameter is small and scale material parameter is large, the critical load of FG nano-plate increases significantly by applying surface effects. As the results show, considering the effects of the surface increases the stiffness of the structure and thus increases the criticality of the structure.

In order to understanding the effect of residual stress on the behavior of buckling load, Fig. 11 is given according to the aspect ratio. It is found that the influence of residual stress on critical load is more obvious at low aspect ratio. The positive and negative residual stress predicts different effect on increasing of critical load. It is due to this fact that the negative and positive residual stresses can be modeled as compressive and tensile loads, respectively. Considering the positive pre-stresses for the piezoelectric nano-sandwich leads to the improvement of the rigidity and stiffness of the structure and as a result, the critical buckling load of the structure increases. By considering the negative pre-stresses, this behavior is exactly reversed.

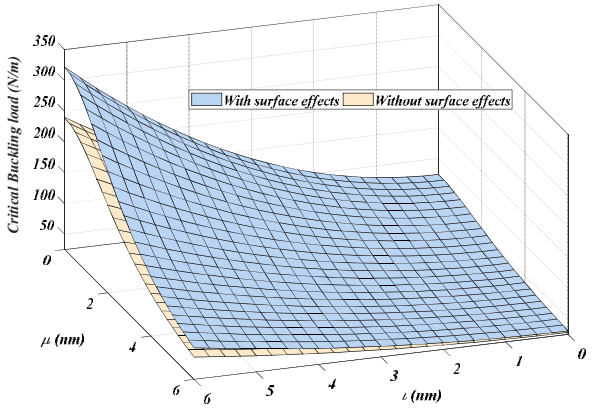

Fig. 10
Variation of critical buckling load versus surface effects.

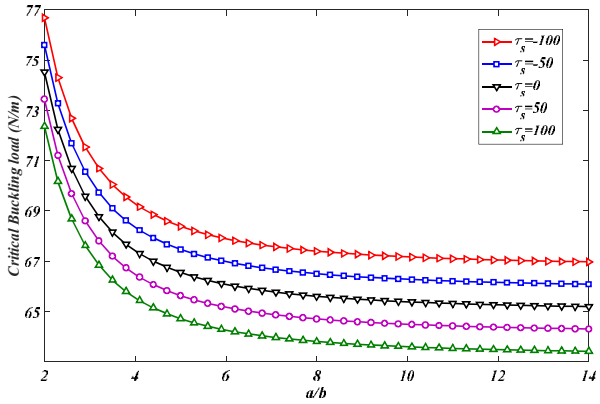

Fig. 11
Influence of residual stress on the buckling load for different aspect ratio.

The behavior of critical load of non-local FG nano-plate with piezoelectric face-sheets based on the surface elasticity theory and quasi-3D theory is plotted in Fig. 12. The results show that the decreasing trend is more prominent at lower ratios of length-to-width. This is due to the fact that presence of surface elastic leads to greater flexural rigidity. In other word, the nano-plate becomes stiffer by taking into account the surface piezoelectricity, which means an increment in the critical load. On the other hand, the assumed quasi-3D theory considers both the effects of shear deformation and stretching and give more accurate results with compared to other shear deformation theory and consequently, the critical load is greatly reducing. According to the obtained results, it can be found that both stretching and surface effects have a significant influence on the critical buckling load that should not be ignored.

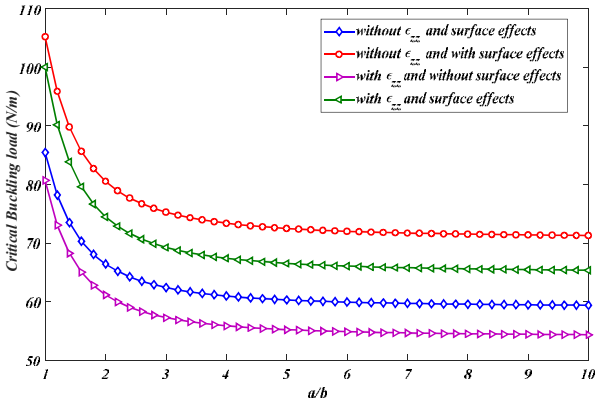

Fig. 12
Stretching and surface effects on buckling critical load of three-layered FG nano-plate.

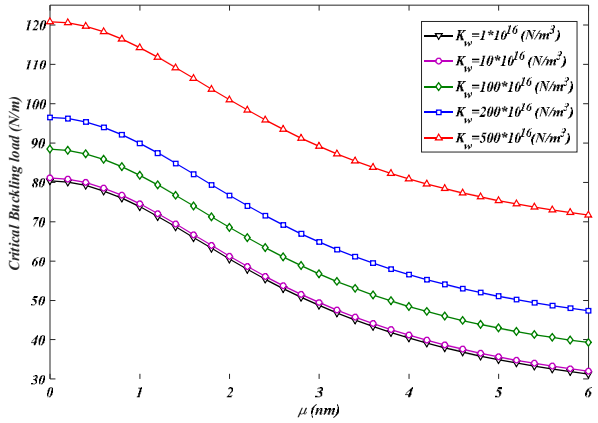

Fig. 13
Critical buckling load of nano-plate in terms of various Winkler coefficients.

The effect of the surrounding elastic medium on critical buckling load of nano-plate versus values the non-local is plotted in Fig. 13. It can be seen that the critical buckling load of nano-plate increases by increasing the Winkler constant. In this range, the stiffness of the FG nano-plate is enhanced due to the increasing of foundation stiffness that leads to an increasing in the total stiffness of the structure. These conditions can be improved with decrease of non-local parameter. Figs. 14 (a) and (b) can be utilized to better understanding of the influences of the orientation of the shear layer and orthotropic foundation on the buckling responses of non-local plate resting on orthotropic Pasternak foundation. In Fig. 14(a), the bi-axial critical load of nano-plate integrated with two piezoelectric layers versus the orthotropy angle is depicted for various Pasternak shear constant. Three-dimensional plot of bi-axial buckling load versus Pasternak shear coefficients in both directions are demonstrated in Fig. 14(b). It can be concluded that increasing k_{gx} and k_{gy} leads to improvement stability of sandwich nano-plate. Thus, the critical buckling load increases. As can be seen from Figs. 14(a)-(b), the orthotropy angle has a significant influence on the variations of critical load. Therefore, it is clearly evident that the effect of both coefficients (k_{gx}, k_{gy}) is the same at $\theta = \pi/4$ and the drawn graph is perfectly symmetrical.

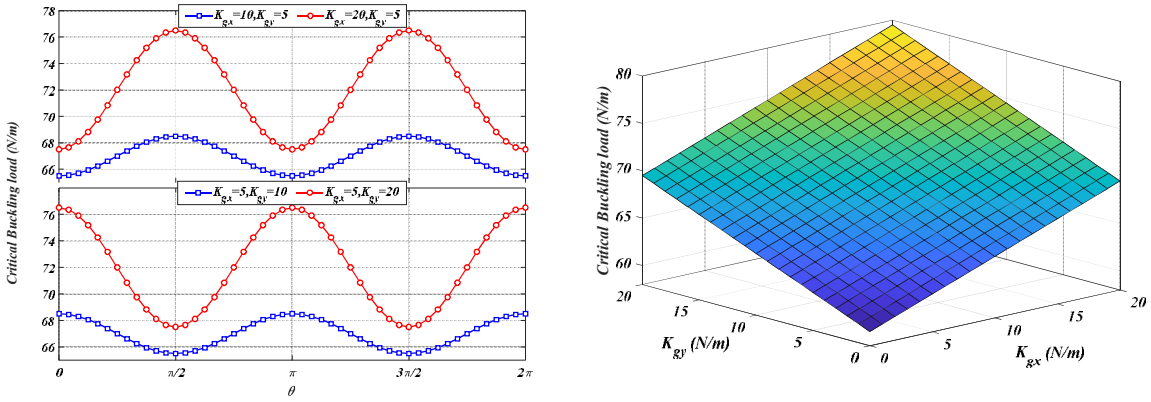

(a) variations of orthotropic angle (b) variations of shear layer coefficients

Fig. 14
Pasternak coefficients effect on buckling load with respect to orthotropic angle.

The critical load of a rectangular FG nano-plate according to the stretching and piezoelectric effects versus small scale parameter is depicted in Fig. 15 for various elastic foundations. As shown in the figure, the buckling load of the rectangular nano-plate increases by considering the elastic medium. This figure shows that the highest critical buckling load is related to the orthotropic medium. It is due to this fact that the Orthotropic Pasternak model is capable to describing both the transverse shear and normal loads of the elastic medium besides that this model is an arbitrarily oriented foundation. It can be understood that the selection of appropriate elastic medium plays an important and decisive role in system stability, since elastic medium makes the system stiffer and more stable.

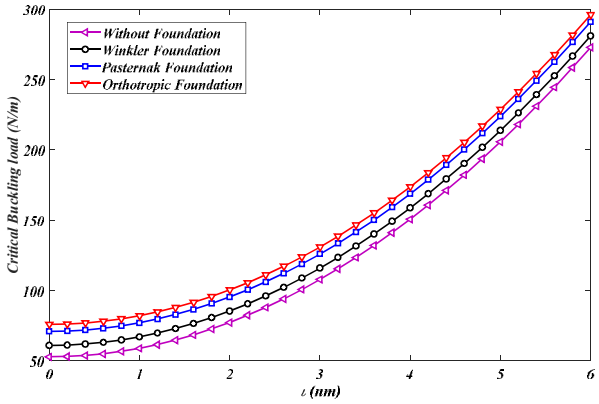

Fig. 15
The effect of different foundation on the critical buckling load.

5 CONCLUSIONS

In this paper, surface effect on the buckling characteristics of three-layered nano-plates including FG core and piezoelectric face-sheets rested on elastic foundation based on NSGT are investigated. In order to extraction of governing equations, a refined plate theory according to the stretching effect is utilized incorporating physical neutral surface concept. An analytical procedure is applied to solve the nonlocal governing equations extracted by Hamilton's principle. Finally, the influences of various parameters such as gradient index, non-locality parameter, elastic medium, geometric ratios, length scale parameter and etc. on buckling responses of FG nano-plate are

investigated. The length scale parameter has an increasing effect on critical load, especially in the lower non-locality parameter. Surface effects play very important role in the increasing critical buckling load of FG nano-structure. These effects are strongly dependent on size parameters. In addition, it can be seen that the stretching effect has a significant efficacy on reducing critical load, especially at higher thicknesses. So that by ignoring the stretching parameter in the low thickness of the nanoplate, major changes in the critical buckling load are not occurred. It can be concluded that the response of buckling analysis with considering surface effects is sensitive for variations of the power-law index and aspect ratio. The presence of orthotropic foundation leads to an essential increment in critical buckling load of the FG nano-plates.

In conclusion, it can understand that the present model is accurate and efficient in predicting critical load of FG nano-plates. This study can provide significant reference in analyzing the mechanical behavior of nano-structure and it is also expected to be useful for designing and improving the nano-smart devices or sensors and actuators.

REFERENCES

[1] Feri M., Krommer M., Alibeigloo A., 2021, Three-dimensional static analysis of a viscoelastic rectangular functionally graded material plate embedded between piezoelectric sensor and actuator layers, *Mechanics Based Design of Structures and Machines* **51(**7): 3843-3867.

[2] Marzavan S., Nastasescu V., 2023, Free vibration analysis of a functionally graded plate by finite element method, *Ain Shams Engineering Journal* **14**(8): 102024.

[3] Frahlia H., Bennai R., Nebab M., Ait Atmane H., Tounsi A., 2022, Assessing effects of parameters of viscoelastic foundation on the dynamic response of functionally graded plates using a novel HSDT theory, *Mechanics of Advanced Materials and Structures* **30**(13): 2765-2779.

[4] Zargar Ershadi M., Faraji Oskouie M., Ansari R., 2022, Nonlinear vibration analysis of functionally graded porous circular plates under hygro-thermal loading, *Mechanics Based Design of Structures and Machines* **52**(2): 1042-1059.

[5] Xie K., Chen H., Wang Y., Li L., Jin F., 2024, Nonlinear dynamic analysis of a geometrically imperfect sandwich beam with functionally graded material facets and auxetic honeycomb core in thermal environment, *Aerospace Science and Technology* **144**: 108794.

[6] Arefi M., Soltan Arani A.H., 2018, Higher order shear deformation bending results of a magnetoelectrothermoelastic functionally graded nanobeam in thermal, mechanical, electrical, and magnetic environments, *Mechanics Based Design of Structures and Machines* **46**(6): 669-692.

[7] Ghorbanpour Arani A., Kolahdouzan F., Abdollahian M., 2018, Nonlocal buckling of embedded magnetoelectroelastic sandwich nanoplate using refined zigzag theory, *Applied Mathematics and Mechanics* **39**(4): 529-546

[8] Singh A.K., Koley S, Negi A., 2022. Remarks on the scattering phenomena of love-type wave propagation in a layered porous piezoelectric structure containing surface irregularity, *Mechanics of Advanced Materials and Structures* **30**(12): 2398-2429.

[9] Dhua S., Mondal S., Maji A., 2024, Surface effects on wave propagation in piezoelectric–piezomagnetic loosely bonded bilayer system using nonlocal theory of elasticity, *thin wall structure* **197**: 111612.

[10] Biswas M., Sahu S.A., 2022, Surface wave dispersion in imperfectly bonded flexoelectric-piezoelectric/FGPM bi-composite in contact of Newtonian liquid, *Mechanics of Advanced Materials and Structures* **30**(14): 2995-3012.

[11] Mirzaei M., 2022, Vibration characteristics of sandwich plates with GPLRC core and piezoelectric face sheets with various electrical and mechanical boundary conditions, *Mechanics Based Design of Structures and Machines* **52**(2): 990-1013.

[12] Hai T., Al-Masoudy M.M., Alsulamy S., El Ouni M.H., Ayvazyan A., Kumar A., 2023, Size-dependent free vibration analysis of honeycomb sandwich microplates integrated with piezoelectric actuators based on the modified strain gradient theory, *Composite Structures* **305**: p.116555.

[13] Ghorbanpour Arani A., Jamali M., Mosayyebi M., Kolahchi R., 2016, Wave propagation in FG-CNT-reinforced piezoelectric composite micro plates using viscoelastic quasi-3D sinusoidal shear deformation theory, *Composites Part B: Engineering* **95**: 209-224.

[14] Cao T.N.T., Reddy J.N., Lieu Q.X., Nguyen X.V., Luong V.H., 2021, A multi-layer moving plate method for dynamic analysis of viscoelastically connected double-plate systems subjected to moving loads, *advanced structural engineering* **24**(9): 1798-1813.

[15] Ragb O., Matbulyb M.S., 2021, Nonlinear vibration analysis of elastically supported multi-layer composite plates using efficient quadrature techniques, *International Journal for Computational Methods in Engineering Science and Mechanics* **23**(2): 129-146.

[16] Taghizadeh S.A., Naghdinasab M., Madadi H., Farrokhabadi A., 2021, Investigation of novel multi-layer sandwich panels under quasi-static indentation loading using experimental and numerical analyses, *Thin wall structure* **160**: 107326.

[17] Amoozgar M., Fazelzadeh S.A., Ghavanloo E., Ajaj R.M., 2022, Free vibration analysis of curved lattice sandwich beams, *Mechanics of Advanced Materials and Structures* **31**(2): 343-355

[18] Sahoo B., Sharma N., Sahoo B., Ramteke P.M., Panda S.K., Mahmoud S.R., 2022, Nonlinear vibration analysis of FGM sandwich structure under thermal loadings, *Structures* **44**: 1392-1402.

[19] Derikvand M., Farhatnia F., Hodges H., 2021, Functionally graded thick sandwich beams with porous core: buckling analysis via differential transform method, *Mechanics Based Design of Structures and Machines* **51**(7): 3650-3677.

[20] Li F., Yuan W., Zhang C., 2021, Free vibration and sound insulation of functionally graded honeycomb sandwich plates, *Journal of Sandwich Structures and Materials* **24**(1): 565-600.

[21] Ghorbanpour Arani A., Shahraki M.E., Haghparast E., 2022, Instability analysis of axially moving sandwich plates with a magnetorheological elastomer core and GNP-reinforced face sheets, *journal of brazilian society of mechanical sciences and engineering* **44**(4):150

[22] Li J., Kardomateas G., Liu L., 2023, Vibration analysis of thick-section sandwich structures in thermal environments, *international journal of mechanical sciences* **241**: 107937.

[23] Liu S., Wang K., Wang B., 2023, Buckling and vibration characteristic of anisotropic sandwich plates with negative Poisson's ratio based on isogeometric analysis, *Mechanics Based Design of Structures and Machines* **9**:1-16.

[24] Ren H., Zhuang X., Oterkus E., Zhu H., Rabczuk T., 2021, Nonlocal strong forms of thin plate, gradient elasticity, magneto-electro-elasticity and phase-field fracture by nonlocal operator method, *Engineering Computations* **39**: 23–44.

[25] Pham Q.H., Nguyen P.C., Tran T.T., 2022, Dynamic response of porous functionally graded sandwich nanoplates using nonlocal higher-order isogeometric analysis, *Composite Structure* **290**: 115565,

[26] Nguyen N.V., Phan D.H., 2023, A refined quasi-3D isogeometric model for dynamic instability of graphene nanoplatelets-reinforced porous sandwich plates, *aerospace science and technology* **142**: 108595.

[27] Hung P.T., Phung-Van P., Thai C.H., 2023, Small scale thermal analysis of piezoelectric–piezomagnetic FG microplates using modified strain gradient theory, *International Journal of Mechanics and Materials in Design* **19**(4): 739-761.

[28] Jin Q., 2021, Interlaminar stress analysis of functionally graded graphene reinforced composite laminated plates based on a refined plate theory, *Mechanics of Advanced Materials and Structures* **29**(25): 4138-4150.

[29] Tharwan M.Y., Daikh A.A., Assie A.E., Alnujaie A., Eltaher M.A., 2023, Refined quasi-3D shear deformation theory for buckling analysis of functionally graded curved nanobeam rested on Winkler/Pasternak/Kerr foundation, *Mechanics Based Design of Structures and Machines* 1-24.

[30] Hai Van N.T., Hong N.T., 2023, Novel finite element modeling for free vibration and buckling analysis of non-uniform thickness 2D-FG sandwich porous plates using refined Quasi 3D theory, *Mechanics Based Design of Structures and Machines* 1-27.

[31] Shahmohammadi M.A., Azhari M., Salehipour H., Thai H.T., 2023, Buckling of multilayered CNT/GPL/fibre/polymer hybrid composite plates resting on elastic support using modified nonlocal first-order plate theory, *Mechanics Based Design of Structures and Machines* **52**(3): 1785-1810.

[32] Ghandourah E.E., Daikh A.A., Alhawsawi A.M, Fallatah O.A., EltaherM.A., 2022, Bending and buckling of FG-GRNC laminated plates via quasi-3D nonlocal strain gradient theory, *Mathematics* **10**(8): 1321

[33] Hung D.X., Van Long N., Tu T.M., Trung D.X., 2024, Bending analysis of FGSP nanoplate resting on elastic foundation by using nonlocal quasi-3D theory, *Thin Wall Structure* **196**: 111510.

[34] Daikh A.A., Belarbi M.O., Khechai A., Li L., Ahmed H.M., Eltaher M.A., 2023, Buckling of bi-coated functionally graded porous nanoplates via a nonlocal strain gradient quasi-3D theory, *Acta Mechanica* **234**(8): 3397-3420.

[35] Shahzad M.A., Sahmani S., Safaei B., Basingab M.S., Hameed A.Z., 2023, Nonlocal strain gradient-based meshless collocation model for nonlinear dynamics of time-dependent actuated beam-type energy harvesters at nanoscale, *Mechanics Based Design of Structures and Machine*s 1-35.

[36] Soleimani A., Zamani F., Haghshenas Gorgani H., 2022, Buckling analysis of three-dimensional functionally graded Euler-Bernoulli nanobeams based on the nonlocal strain gradient theory, *Journal of Applied and Computational Mechanics* **53**(1): 24-40.

[37] Li L., Hu Y., Ling L., 2015, Flexural wave propagation in small-scaled functionally graded beams via a nonlocal strain gradient theory, *Composite Structure* **133**: 1079-1092.

[38] Jalaei M.H., Civalek Ö.M.E.R., 2019, A nonlocal strain gradient refined plate theory for dynamic instability of embedded graphene sheet including thermal effects, *Composite Structure* **220**: 209-220.

[39] Ebrahimi F., Dabbagh A., 2017, On flexural wave propagation responses of smart FG magneto-electro-elastic nanoplates via nonlocal strain gradient theory, *Composite Structure* **162**: 281-293.

[40] Ma L.H., Ke L., Reddy J.N., Yang J., Kitipornchai S., Wang Y.S., 2018, Wave propagation characteristics in magneto-electro-elastic nanoshells using nonlocal strain gradient theory, *Composite Structure* **199**: 10-23.

[41] Sahmani S., Aghdam M.M., Rabczuk T., 2018, Nonlinear bending of functionally graded porous micro/nano-beams reinforced with graphene platelets based upon nonlocal strain gradient theory, *Composite Structure* **186**: 68-78.

[42] Jamali M., Shojaee T., Mohammadi B., 2020, Analytical buckling and post-buckling characteristics of Mindlin micro composite plate with central opening by use of nonlocal elasticity theory, *Journal of Applied and Computational Mechanics* **51**(1): 231-238.

[43] Barati M.R., Shahverdi H., 2017, An analytical solution for thermal vibration of compositionally graded nanoplates with arbitrary boundary conditions based on physical neutral surface position, *Mechanics of Advanced Materials and Structures* **24**(10): 840-853.

[44] Bellifa H., Benrahou K.H., Hadji L., Houari M.S.A., Tounsi A., 2016, Bending and free vibration analysis of functionally graded plates using a simple shear deformation theory and the concept the neutral surface position, *Journal of the Brazilian Society of Mechanical Sciences and Engineering* **38**(1): 265-275.

[45] Farzam-Rad S.A., Hassani B., Karamodin A., 2017, Isogeometric analysis of functionally graded plates using a new quasi-3D shear deformation theory based on physical neutral surface, *Composites Part B: Engineering* **108**: 174-189.

[46] Barati A., Norouzi S., 2020, Nonlocal elasticity theory for static torsion of the bi-directional functionally graded microtube under magnetic field, *Journal of Applied and Computational Mechanics* **51**(1): 30-36.

[47] Ghorbanpour-Arani A.A., Khoddami Maraghi Z., Ghorbanpour Arani A., 2023, The Frequency Response of Intelligent Composite Sandwich Plate Under Biaxial In-Plane Forces, *Journal of Solid Mechanic* **15**(1): 1-18.

[48] Mahmoudi A., Benyoucef S., Tounsi A., Benachour A., Adda Bedia E.A., Mahmoud, S.R., 2019, A refined quasi-3D shear deformation theory for thermo-mechanical behavior of functionally graded sandwich plates on elastic foundations, *Journal of Sandwich Structures and Materials* **21**(6): 1906-1929.

[49] Meziane M.A.A., Abdelaziz H.H., Tounsi A., 2014, An efficient and simple refined theory for buckling and free vibration of exponentially graded sandwich plates under various boundary conditions, *Journal of Sandwich Structures and Materials* **16**(3): 293-318.

[50] El Meiche N., Tounsi A., Ziane N., Mechab I., 2011, A new hyperbolic shear deformation theory for buckling and vibration of functionally graded sandwich plate, *International Journal of Mechanical Sciences* **53**(4): 237-247.

[51] Ghorbanpour Arani A., Zarei H.B.A., Haghparast E., 2018, Vibration response of viscoelastic sandwich plate with magnetorheological fluid core and functionally graded-piezoelectric nanocomposite face sheets, *Journal of Vibration and Control* **24**(21): 5169-5185.

[52] Ghorbanpour Arani A., Haghparast E., Zarei H.B.A., 2016, Nonlocal vibration of axially moving graphene sheet resting on orthotropic visco-Pasternak foundation under longitudinal magnetic field, *Physica B: Condensed Matter* **495:** 35-49.

[53] Alipour M.M., Shariyat M., 2011, A power series solution for free vibration of variable thickness Mindlin circular plates with two-directional material heterogeneity and elastic foundations, *Journal of Solid Mechanics* **3**(2): 183-197.

[54] Najafizadeh M.M., Raki M., Yousefi P., 2018, Vibration analysis of FG nanoplate based on third-order shear deformation theory (TSDT) and nonlocal elasticity, *Journal of Solid Mechanics* **10**(3):464-475.

[55] Molla-Alipour M., Shariyat M., Shaban M., 2020, Free vibration analysis of bidirectional functionally graded conical/cylindrical shells and annular plates on nonlinear elastic foundations, based on a unified differential transform analytical formulation, *Journal of Solid Mechanics* **12**(2): 385-400.

[56] Ghorbanpour Arani A., Haghparast E., Zarei, H.B.A., 2016, Vibration of axially moving 3-phase CNTFPC plate resting on orthotropic foundation, *Structural Engineering and Mechanics* **57**(1): 105-126.

[57] Thai H.T., Vo T.P., 2013. A new sinusoidal shear deformation theory for bending, buckling, and vibration of functionally graded plates. *Applied mathematical modelling* **37**(5): 3269-3281.

[58] Shufrin I., Eisenberger M., 2005, Stability and vibration of shear deformable plates—first order and higher order analyses. *International Journal of Solids and Structures* **42**(3-4): 1225-1251.

[59] Haghparast E., Ghorbanpour-Arani A., Ghorbanpour Arani A., 2020. Effect of fluid–structure interaction on vibration of moving sandwich plate with Balsa wood core and nanocomposite face sheets. *International Journal of Applied Mechanics* ***12***(07): 2050078.